SIGMA: A weather radar signal fluctuation descriptor for ground clutter identification

Corentin Lubeigt

***Abstract*—Weather radar signal fluctuation has been used to identify ground clutter (GC) from meteorological echoes for decades. Indeed, the fluctuation of a radar signal intuitively informs whether an echo comes from a static object (GC) or a random phenomenon (precipitation). Based on this intuition, Météo-France has implemented the clutter indicator, Ci, which proved satisfactory to correctly identify pixels affected by GC. In this study, a revision of the Ci, noted Σ, is presented. The theoretical statistics (mean and variance) of Σ are then derived in the case of meteorological echoes with large spectral width and verified with both simulated and real data. As an example this result is then used to set the false alarm rate of a GC detector.**

***Index Terms*—Weather radar, signal fluctuation, ground clutter identification**

I. Introduction

WEATHER radars are crucial in many weather agencies as they provide global rainfall observations completing more local measurements such as rain gauges. However, radar data is always corrupted with various non-meteorological echoes: interferences, speckle noise, insects, birds and ground clutter (GC). The latter is of particular interest as it affects precious data close to the ground [1]. Paradoxically, GC is not a static problem when anomalous propagation (AP) occurs [2]: in certain atmospheric conditions, GC location may vary making it difficult for the user to rely on static clutter maps.

Apart from a judicious choice of radar location, there are two ways to limit the effect of GC: i) by implementing ground clutter filters (GCF) on raw samples and ii) by post-processing the aggregated radar products via classification algorithms.

GCF have been thoroughly studied since the arrival of Doppler radars. Thanks to its spectral properties: located around zero mean radial velocity and narrow spectrum [3], a straightforward solution to remove GC is then to apply a notch filter [4], [5]. However simple, this approach can deteriorate weather signals if their mean radial velocity are close to zero. To fix this, one can, for instance, detect and apply the filter only when there is GC [6] or reconstruct the filtered spectrum via regression [7]. Other approaches focus on the properties of the signal auto-correlation function (ACF) to separate the weather signal from the GC [8].

Post-processing solutions aim at distinguishing pixels polluted by GC from weather signals in order to censor them. The general idea is to find one or several parameters that discriminate GC from weather signals. A typical approach is to look at the statistical behavior of the pulse-to-pulse power fluctuation [9]–[11]. Recently [12] presented a promising phase fluctuation index that is robust to zero-mean radial velocity weather signals. These fluctuations can often be associated to other products (e.g., textures, polarimetric variables) to feed a fuzzy logic algorithm or neural networks [13].

Météo-France radars are using a staggered scheme with 3 pulse repetition times (PRT) [14] making it difficult to implement GCF. Consequently, GC identification has been done for years [15] using a pulse-to-pulse reflectivity fluctuation called clutter indicator Ci [10]. This indicator, adapted to staggered schemes, is dynamic, robust to both AP and intense rain over GC. It is used as a main parameter in a fuzzy logic algorithm.

In this study, a revision of Ci is presented. This product called Σ is more robust to weak signals. The statistical properties of Σ are investigated in the case of rain only, leading to a closed-form formula of its mean and variance. Such results are confirmed with both simulated and real data. An application of this result is finally proposed to build a GC identification routine with constant false alarm rate (CFAR).

II. Definition

A. Recall of the clutter indicator Ci

In [10], Ci was introduced as the averaged fluctuation of the signal within a range gate, separated by a delay τ. The k-th pulse fluctuation, noted Δ_k, was defined as follows:

$$\Delta_k = 10\left|\log_{10}(P_k) - \log_{10}(P_{k-\tau})\right|, \tag{1}$$

where P_k is the estimated power from the k-th pulse. Ci (in dB) is the averaged fluctuation over M samples:

$$Ci = \frac{1}{M-1}\sum_{k=1}^{M}\Delta_k. \tag{2}$$

As mentioned in [15], this indicator has been used in Météo-France for ground-clutter identification. This parameter is connected to the signal ACF evaluated at lag τ: a signal strongly correlated with itself such as a ground echo will have a small Ci and rapidly varying signals such as rain echoes will output larger signal fluctuations and Ci. It was shown in [10] that the choice of the lag τ is crucial to properly distinguish GC from meteorological echoes.

B. Definition of Σ

Ci has been revisited to be more robust to weak weather signals such as in the precipitation cells edges. This was done by weighting the signal fluctuation by the received power:

$$\Sigma = \frac{\sum_{k=1}^{M} P_k\Delta_k}{\sum_{k=1}^{M} P_k}, \tag{3}$$

where Δ_k is defined in (1) and Σ is expressed in dB. This definition was meant to homogenize the value of Σ over precipitation cells.

C. Lubeigt is with Météo-France, 31057, Toulouse, France, e-mail: corentin.lubeigt@meteo.fr

C. Illustration

The situation from Météo-France C-band radar located in Toulouse, presented hereafter, will be used for the rest of this study. The situation occurred in May 19, 2025 at 15:00 UTC and was seen by the radar at an elevation of 1.5°.

The staggered scheme in used at Météo-France allows a wide extended Nyquist interval with low duty cycle. Toulouse radar is using the set of pulse repetition frequencies (PRF) 440/489/550 Hz and for the computation of the signal fluctuation (1), τ is the sum of the 3 PRT: 6.14 ms. In practice, to evaluate Δ_k, the sample k is compared to the sample $k-3$.

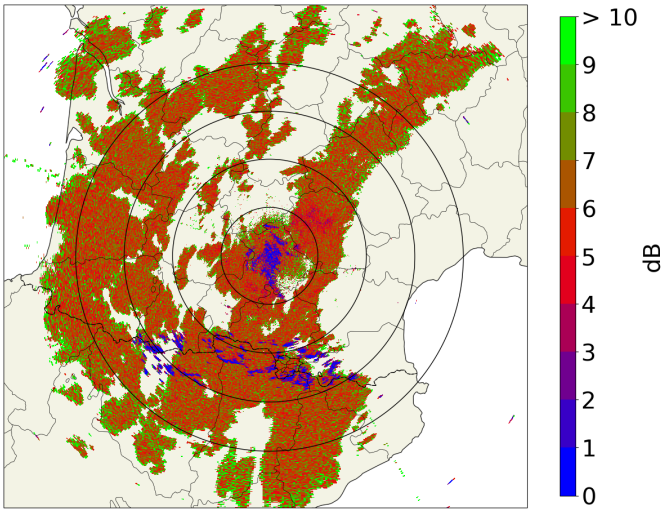

Fig. 1. Clutter indicator Ci for the situation of May 19, 2025 at 15:00 UTC seen by C-band Toulouse radar at elevation 1.5°.

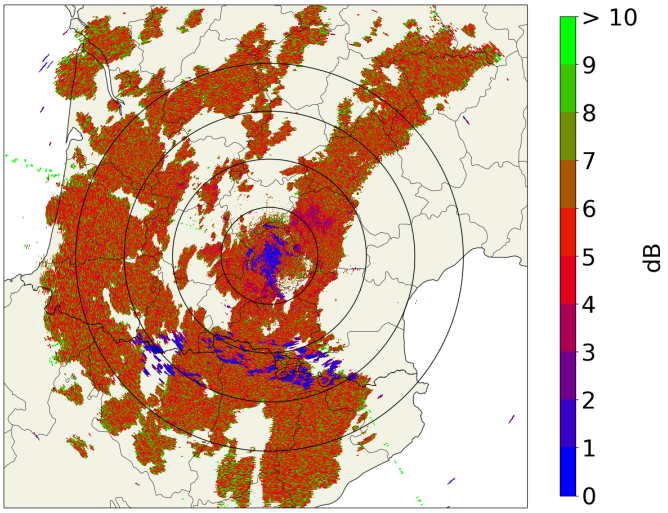

Fig. 2. Σ for the situation of May 19, 2025 at 15:00 UTC seen by C-band Toulouse radar at elevation 1.5°.

Fig. 1 and Fig. 2 represent the plan position indicator (PPI) for the above-mentioned situation where Ci and Σ (respectively) are computed. On both figures, the ground echoes appear clearly in blue around the radar and in the south where the radar beam hits the Pyrenees range. Most of the other pixels take a value around 6dB. The main difference between these figures can be seen at the edge of the precipitation cells where Ci takes more high values (> 10 dB) than Σ. In Fig. 3,

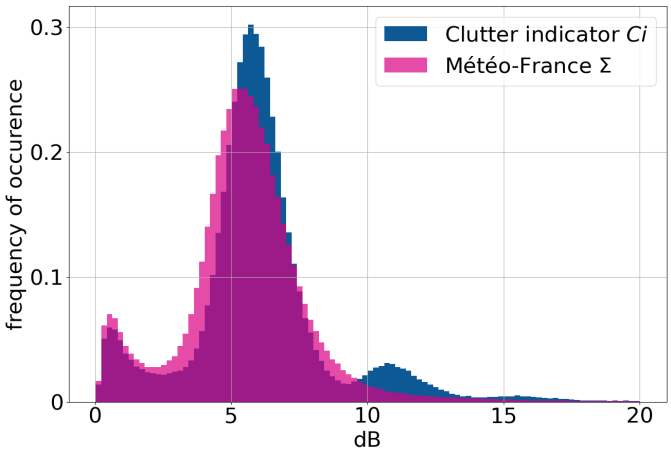

Fig. 3. Normalized histogram of Ci and Σ for the situation of May 19, 2025 at 15:00 UTC seen by C-band Toulouse radar at elevation 1.5°.

the mode located around 11 dB for Ci disappears for Σ, leaving only two main modes: around 1 dB for GC and around 6 dB for weather echoes. The rest of this study will focus on Σ.

III. Statistical behavior in rain

Based on Fig. 3, a well chosen threshold on Σ should help identifying pixels polluted by GC. Hereafter, the theoretical statistical behavior of Σ is investigated to determine how to fix this threshold.

A. Signal model

Let I_k and Q_k be the k-th sample in-phase and quadrature components of the complex signal [16, Chap. 2] and $P_k = |X_k|^2 = I_k^2 + Q_k^2$ the corresponding power. Following are the main assumptions on the signal model for this study:

- I_k and Q_k are Gaussian so that P_k has a scaled χ^2 distribution with 2 degrees of freedom (DOF) with a scale factor $\sigma_P/2$ that includes the signal and noise powers: $P_k = \frac{\sigma_P}{2} u_k$ and $P_{k-\tau} = \frac{\sigma_P}{2} v_k$ where u_k and v_k are χ^2 distributed with 2 DOF,
- the Doppler power spectrum is assumed Gaussian [3, Chap. 6] with a given spectral width σ_v. Consequently, the normalized amplitude of the signal ACF is Gaussian: $\rho_s(\tau) = \exp\left(-\tau^2/2\sigma_\tau^2\right)$, where $\sigma_\tau = \lambda/(4\pi\sigma_v)$ and λ is the signal carrier wavelength.
- spectral width is considered large so that P_k and $P_{k-\tau}$ are uncorrelated. For $\sigma_v = 1$ m/s, the corresponding correlation coefficient between P_k and $P_{k-\tau}$ for Toulouse C-band radar ($\tau = 6.14$ ms) is $\rho_s(\tau)^2 = 0.12$. Typical echoes in rain have large σ_v [17] so that the power samples spaced by τ can be considered independent.

With the previous assumptions, (3) can be recast as follows:

$$\Sigma = \frac{10}{\ln(10)} \frac{\frac{1}{M}\sum_{k=1}^{M} u_k \left|\ln\left(\frac{u_k}{v_k}\right)\right|}{\frac{1}{M}\sum_{k=1}^{M} u_k} \triangleq \frac{10}{\ln(10)} \frac{\Sigma_n}{\Sigma_d}, \qquad (4)$$

where Σ_n and Σ_d are random variables corresponding to the numerator and the denominator (respectively) of Σ.

B. Evaluation of the mean and the standard deviation of Σ

Based on (4), Σ is the ratio of two mean estimations. According to the central limit theorem, considering M large, both Σ_n and Σ_d can be seen Gaussian whose mean and variance can be computed:

- Σ_n: mean ≈ 2.773, variance $\approx 21.432/M$ (see Appendix A and [18]),
- Σ_d: mean = 2, variance = $4/M$ (u_k having a χ^2 distribution with 2 DOF).

Unsurprisingly, Σ_n and Σ_d are correlated and this has to be taken into account to evaluate the moments of Σ. It can be shown that the correlation coefficient between Σ_n and Σ_d, denoted ρ, is constant when the σ_v is large enough and the value of this correlation coefficient can be evaluated as: $\rho \approx 0.599$ (see Appendix B and [18]).

Finally, an approximation of the mean and variance of Σ is obtained using the Delta method (see Appendix C). In case of rain with large σ_v, this parameter has the following moments:

$$\mathrm{E}\{\Sigma\} \approx \frac{10}{\ln(10)} \frac{\mathrm{E}\{\Sigma_n\}}{\mathrm{E}\{\Sigma_d\}} = 10\log_{10}(4) = 6 \text{ dB}. \quad (5)$$

$$\mathrm{Var}\{\Sigma\} \approx 64.798/M \text{ (dB)}^2, \ \mathrm{SD}\{\Sigma\} \approx 8.05/\sqrt{M} \text{ dB}. \quad (6)$$

where SD{·} denotes the standard deviation operator.

IV. Validation

In order to confirm the results obtained in Section III, the theoretical mean and variance of Σ are compared with both simulated and real data. In both cases, the estimated Σ (using (3)) is compared to the estimated spectral width $\widehat{\sigma}_v$ using:

$$\widehat{\sigma}_v = \frac{1}{3}\sum_{i=1}^{3} \frac{\lambda}{2\sqrt{2}\pi \mathrm{PRT}_i} \sqrt{\ln\left(\widehat{R}_i(0)/\widehat{R}_i(1)\right)}, \quad (7)$$

where $\widehat{R}_i(k)$ is the estimated signal ACF evaluated at lag k with pulse-pairs spaced by PRT_i.

A. Simulation

Weather radar signals are simulated using the method detailed in [19]. The following figures are obtained considering a signal to noise ratio of 20 dB, a mean radial velocity of 0 m/s and a spectral width varying between 0.01 to 5 m/s. The signal is then sampled with the 3-PRT staggered scheme. The number of samples is set to $M = 42$ which correspond to an azimuthal span of 0.5° for low elevation scans. For each spectral width value, 2000 Monte Carlo simulations are run and both Σ and $\widehat{\sigma}_v$ are computed. Fig. 4 represents the 2D histogram of Σ and $\widehat{\sigma}_v$ and Fig. 5 represents the corresponding mean and variance of Σ for each $\widehat{\sigma}_v$ value.

In Fig. 4 and Fig. 5, the evolution of the distribution of Σ can be divided in two regions.

- For $\sigma_v > 1$ m/s (rain echoes), the correlation between P_k and $P_{k-\tau}$ is close to zero, Σ has then the saturated behavior predicted by the results obtain in the previous sections. This is especially clear for the mean.
- For $\sigma_v < 1$ m/s (GC), the correlation is not zero and Σ rapidly decreases with σ_v.

In Fig. 5, the estimated standard deviation converges to the theoretical value at 3 m/s. Between 1 m/s and 3 m/s, the assumption of independent samples does not hold so well as mentioned in Sec. III-A and terms should be added in the covariances (16) and (20) evaluated in the appendices. As σ_v is getting small, the computation gets more tedious. For this reason, the contribution of this study restricts itself to the asymptotic case of large σ_v.

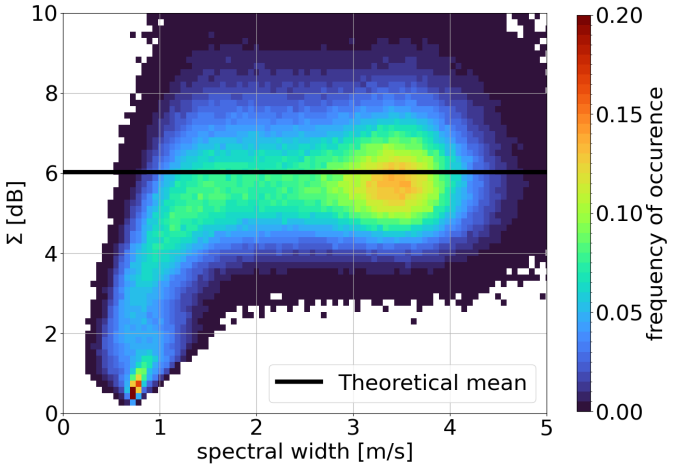

Fig. 4. Σ – σ_v plot based on simulated weather radar signals.

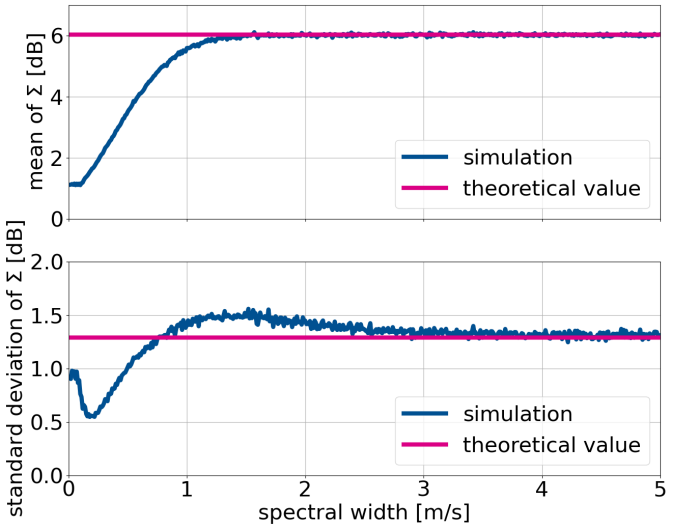

Fig. 5. Estimated moments of Σ with regard to the spectral width: on top is the mean, on the bottom is the standard deviation.

B. Real data

Toulouse radar situation presented in Sec. II-C is now considered to see how the estimated Σ and σ_v on real data compare. Fig. 6 shows strong similarities with Fig. 4 with a saturated value around 6 dB when the estimated spectral width is large. This is confirmed in Fig. 7 where the estimated mean and standard deviation converge to their theoretical value.

Difference for small σ_v and for large Σ are due to cases that were not taken into account in the assumptions: interference, clear air echoes, mix of weather echoes with GC. Besides, in Fig. 7, the estimated standard deviation is noisy for large σ_v

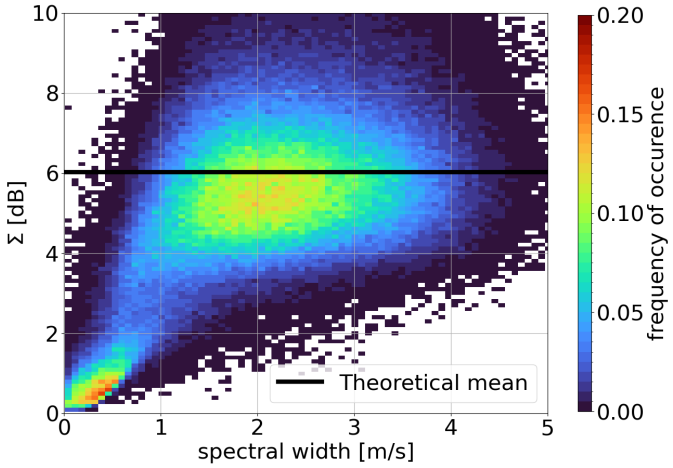

Fig. 6. Σ – σ_v plot for the situation of May 19, 2025 at 15:00 UTC seen by C-band Toulouse radar at elevation 1.5°.

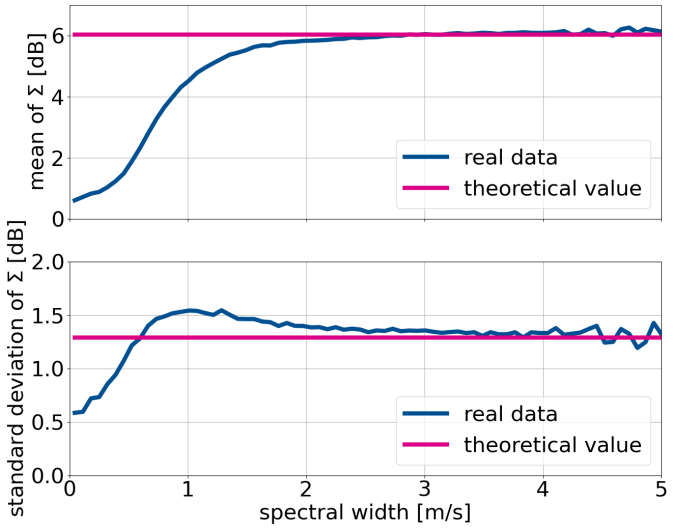

Fig. 7. Estimated moments of Σ with regard to the spectral width: on top is the mean, on the bottom is the standard deviation.

as there are fewer pixels presenting this spectral width in the considered dataset.

V. Application for Ground Clutter Identification

An application of the results obtained in Section III is to build a GC detection test with a threshold t fixed by a chosen probability of false alarm p_{fa}.

- H_0: $\Sigma > t$, the echo is not from ground clutter,
- H_1: $\Sigma < t$, the echo is from ground clutter.

Under the null hypothesis H_0, thanks to the central limit theorem when M is large, Σ has a Gaussian distribution with mean $\mu_\Sigma = 6$ dB and standard deviation $\sigma_\Sigma = 8.05/\sqrt{M}$.

Fixing the p_{fa} corresponds to fixing a threshold t to which the test statistics (here the estimated Σ) is compared:

$$p_{\text{fa}} = \mathrm{P}\left[\text{reject } H_0 | H_0\right] = \mathrm{P}\left[\Sigma < t | \Sigma \sim \mathcal{N}\left(\mu_\Sigma, \sigma_\Sigma^2\right)\right], \quad (8)$$

where $\mathrm{P}[\cdot]$ stands for *probability of*. Manipulations of (8) lead to $t = \mu_\Sigma + \sigma_\Sigma \Phi^{-1}(p_{\text{fa}})$, where $\Phi^{-1}(\cdot)$ is the inverse of the cumulative distribution function of a unit normal distribution.

As an example, $M = 42$ and $p_{\text{fa}} = 0.05$ lead to $t = 3.98$ dB which is sufficient as a first step prior to a more selective fuzzy logic classification as it is done at Météo-France.

VI. Conclusion

In this study, a radar product, called Σ, used for GC classification has been recalled with a revision more robust at low SNR. Based on assumptions on the weather radar signal Doppler spectrum, the first two moments of Σ have been derived and checked by both simulation and radar data. Finally, a typical application of this result has been illustrated by defining a GC detection test with a fixed false alarm rate.

Σ is a key parameter for classification in Météo-France radar data processing. The knowledge of its statistical behavior allows a better understanding of its reliability. Further work will focus on the characterization of this product when the assumptions of the present study are not valid, that is, when the spectrum is not Gaussian (e.g., in presence of GC and weather signal, of noise only or when interference occurs).

Appendix A
Details on the Numerator of Σ

Details are given on the mean and the variance of Σ_n.

1) Mean of Σ_n: from (4), the expectation of Σ_n is:

$$\mathrm{E}\{\Sigma_n\} = \tfrac{1}{M} E\left\{\textstyle\sum_{k=1}^{M} u_k \left|\ln\left(\frac{u_k}{v_k}\right)\right|\right\} = E\left\{u\left|\ln\left(\tfrac{u}{v}\right)\right|\right\}, \quad (9)$$

u, v are independent χ^2 variables and $\mathrm{E}\{\cdot\}$ is the expectation.

$$E\left\{u\left|\ln\left(\tfrac{u}{v}\right)\right|\right\} = \int_{\mathbb{R}^+}\int_{\mathbb{R}^+} u\left|\ln\left(\tfrac{u}{v}\right)\right| p(u)p(v)\mathrm{d}v\mathrm{d}u, \quad (10)$$

where $p(\cdot)$ is the corresponding probability density functions. All computations done [18, Sec. 2], the mean of Σ shrinks to:

$$\mathrm{E}\{\Sigma_n\} = \mu_\Sigma = 4\ln(2) \approx 2.773. \quad (11)$$

2) Variance of Σ_n: the terms in the sum of Σ_n are independent except for the pairs 3 indexes apart where there is a common variable. Hence, from (4), the variance of Σ_n is:

$$\begin{aligned}\mathrm{Var}\{\Sigma_n\} = \tfrac{1}{M^2}\mathrm{Var}\left\{\textstyle\sum_{k=1}^{M} u_k\left|\ln\left(\frac{u_k}{v_k}\right)\right|\right\} = \tfrac{1}{M}\mathrm{Var}\left\{u\left|\ln\left(\tfrac{u}{v}\right)\right|\right\} \\ + 2\tfrac{M-3}{M^2}\mathrm{Cov}\left\{u\left|\ln\left(\tfrac{u}{v}\right)\right|, w\left|\ln\left(\tfrac{w}{u}\right)\right|\right\},\end{aligned} \quad (12)$$

where $\mathrm{Var}\{\cdot\}$ and $\mathrm{Cov}\{\cdot,\cdot\}$ denote the variance and covariance operators, respectively. For the variance:

$$\mathrm{Var}\left\{u\left|\ln\left(\tfrac{u}{v}\right)\right|\right\} = \mathrm{E}\left\{\left(u\ln\left(\tfrac{u}{v}\right)\right)^2\right\} - \left(\mathrm{E}\left\{u\left|\ln\left(\tfrac{u}{v}\right)\right|\right\}\right)^2. \quad (13)$$

The last term of (13) has already been computed and the first term is obtained by evaluating the following integral:

$$E\left\{\left(u\ln\left(\tfrac{u}{v}\right)\right)^2\right\} = \int_{\mathbb{R}^+}\int_{\mathbb{R}^+}\left(u\ln\left(\tfrac{u}{v}\right)\right)^2 p(u)p(v)\mathrm{d}v\mathrm{d}u. \quad (14)$$

The evaluation of this integral can be obtained [18, Sec. 3]:

$$E\left\{\left(u\ln\left(\tfrac{u}{v}\right)\right)^2\right\} = 8 + 8\tfrac{\pi^2}{3} \approx 34.319. \quad (15)$$

For the covariance:

$$\begin{aligned}\mathrm{Cov}\left\{u\left|\ln\left(\tfrac{u}{v}\right)\right|, w\left|\ln\left(\tfrac{w}{u}\right)\right|\right\} = \mathrm{E}\left\{uw\left|\ln\left(\tfrac{u}{v}\right)\right|\left|\ln\left(\tfrac{w}{u}\right)\right|\right\} \\ - \mathrm{E}\left\{u\left|\ln\left(\tfrac{u}{v}\right)\right|\right\}\mathrm{E}\left\{w\left|\ln\left(\tfrac{w}{u}\right)\right|\right\}.\end{aligned} \quad (16)$$

The last term of (16) has already been computed and the first term is obtained by evaluating the following integral:

$$\begin{aligned}&\mathrm{E}\left\{uw\left|\ln\left(\tfrac{u}{v}\right)\right|\left|\ln\left(\tfrac{w}{u}\right)\right|\right\} = \\ &\int_{\mathbb{R}^+}\int_{\mathbb{R}^+}\int_{\mathbb{R}^+} uw\left|\ln\left(\tfrac{u}{v}\right)\right|\left|\ln\left(\tfrac{w}{u}\right)\right| p(u)p(v)p(w)\mathrm{d}w\mathrm{d}v\mathrm{d}u.\end{aligned} \tag{17}$$

After computation [18, Sec. 6], the integral can be evaluated:

$$\begin{aligned}\mathrm{E}\left\{uw\left|\ln\left(\tfrac{u}{v}\right)\right|\left|\ln\left(\tfrac{w}{u}\right)\right|\right\} &= 2\pi^2 - 32\mathrm{Li}_2\left(\tfrac{1}{3}\right) + \tfrac{35}{24} \\ &- \left(4\ln\left(\tfrac{3}{2}\right) + \tfrac{3}{2}\right)^2 - 2\left(\ln(4) + \tfrac{1}{4}\right)^2 \approx 5.088,\end{aligned} \tag{18}$$

where $\mathrm{Li}_2(\cdot)$ is the polylogarithm.

Finally, putting (15) and (18) together, for a large M the variance of Σ_n, in the case of rain, can be expressed as:

$$\mathrm{Var}\{\Sigma_n\} \approx 21.432/M. \tag{19}$$

Appendix B
Details on the correlation between the numerator and the denominator of Σ

Hereafter, the covariance between Σ_n and Σ_d is evaluated.

$$\begin{aligned}\mathrm{Cov}\left\{\Sigma_n, \Sigma_d\right\} &= \tfrac{1}{M^2}\sum_{i=1}^{M}\sum_{j=1}^{M}\mathrm{Cov}\left\{u_i\left|\ln\left(\tfrac{u_i}{v_i}\right)\right|, u_j\right\} \\ &= \tfrac{1}{M}\mathrm{Cov}\left\{u\left|\ln\left(\tfrac{u}{v}\right)\right|, u\right\} + \tfrac{M-3}{M^2}\mathrm{Cov}\left\{u\left|\ln\left(\tfrac{u}{v}\right)\right|, v\right\}.\end{aligned} \tag{20}$$

Samples are independent so the covariance in the double sum are all null except for $i = j$ and for $i = j+3$ (because $v_i = u_{i-3}$).

$$\mathrm{Cov}\left\{u\left|\ln\left(\tfrac{u}{v}\right)\right|, u\right\} = \mathrm{E}\left\{u^2\left|\ln\left(\tfrac{u}{v}\right)\right|\right\} - \mathrm{E}\left\{u\left|\ln\left(\tfrac{u}{v}\right)\right|\right\}\mathrm{E}\left\{u\right\}, \tag{21}$$

$$\mathrm{Cov}\left\{u\left|\ln\left(\tfrac{u}{v}\right)\right|, v\right\} = \mathrm{E}\left\{uv\left|\ln\left(\tfrac{u}{v}\right)\right|\right\} - \mathrm{E}\left\{u\left|\ln\left(\tfrac{u}{v}\right)\right|\right\}\mathrm{E}\left\{v\right\}. \tag{22}$$

Last terms of each covariance are product of known expectations. First terms are obtained by evaluating (23) and (24).

$$\mathrm{E}\left\{u^2\left|\ln\left(\tfrac{u}{v}\right)\right|\right\} = \int_{\mathbb{R}^+}\int_{\mathbb{R}^+} u^2\left|\ln\left(\frac{u}{v}\right)\right| p(u)p(v)\mathrm{d}v\mathrm{d}u, \tag{23}$$

$$\mathrm{E}\left\{uv\left|\ln\left(\tfrac{u}{v}\right)\right|\right\} = \int_{\mathbb{R}^+}\int_{\mathbb{R}^+} uv\left|\ln\left(\frac{u}{v}\right)\right| p(u)p(v)\mathrm{d}v\mathrm{d}u, \tag{24}$$

Again, these integrals can be evaluated [18, Sec. 4 and 5]:

$$\mathrm{E}\left\{u^2\left|\ln\left(\frac{u}{v}\right)\right|\right\} = 16\ln(2) + 2, \tag{25}$$

$$\mathrm{E}\left\{uv\left|\ln\left(\frac{u}{v}\right)\right|\right\} = 8\ln(2) - 2, \tag{26}$$

Putting all the terms together, the correlation coefficient is:

$$\rho = \frac{\mathrm{Cov}\{\Sigma_n, \Sigma_d\}}{\sqrt{\mathrm{Var}\{\Sigma_n\}\mathrm{Var}\{\Sigma_d\}}} \approx 0.599. \tag{27}$$

Appendix C
Details on the ratio of two correlated Gaussian distributed random variables

Here, details are provided on an approximation of the ratio of two correlated random variables using the Delta method. Let $\mathbf{b}$ be a bivariate Gaussian random variable.

$$\mathbf{b} = \begin{bmatrix} x \\ y \end{bmatrix} \sim \mathcal{N}\left(\begin{bmatrix} \mu_x \\ \mu_y \end{bmatrix}, \begin{bmatrix} \sigma_x^2 & \rho\sigma_x\sigma_y \\ \rho\sigma_x\sigma_y & \sigma_y^2 \end{bmatrix}\right) \tag{28}$$

Then, considering a first order Taylor expansion of $h(\mathbf{b}) = x/y$:

$$\mathrm{E}\left\{h(\mathbf{b})\right\} \approx \frac{\mu_x}{\mu_y}, \tag{29}$$

$$\mathrm{Var}\left\{h(\mathbf{b})\right\} \approx \left(\frac{\mu_x}{\mu_y}\right)^2\left(\frac{\sigma_x^2}{\mu_x^2} + \frac{\sigma_y^2}{\mu_y^2} - 2\rho\frac{\sigma_x\sigma_y}{\mu_x\mu_y}\right). \tag{30}$$

Acknowledgment

The author would like to thank H. Beekhuis for his kind bibliographical hints and Météo-France radar R&D team for the many suggestions that helped improving this document.

References

[1] K. Friedrich, M. Hagen, and T. Einfalt, "A quality control concept for radar reflectivity, polarimetric parameters, and Doppler velocity," *J. Atmos. Oceanic Technol.*, vol. 23, no. 7, pp. 865–887, 2006.
[2] J. A. Pamment and B. J. Conway, "Objective identification of echoes due to anomalous propagation in weather radar data," *J. Atmos. Oceanic Technol.*, vol. 15, no. 1, pp. 98–113, 1998.
[3] R. J. Doviak and D. S. Zrnić, *Doppler radar and weather observations*, 2nd ed. Mineola, NY, USA: Dover Publications, Inc., 2006.
[4] J. N. Chrisman, D. M. Rinderknecht, and R. S. Hamilton, "WSR-88D clutter suppression and its impact on meteorological data interpretation," in *First WSR-88D User's Conference*, Norman, OK, USA, Jan. 1995, pp. 9–20. [Online]. Available: www.roc.noaa.gov/public-documents/operations-branch/Legacy_Clutter_paper.pdf
[5] H. Leijnse, H. Beekhuis, and I. Holleman, "Doppler clutter removal on KNMI weather radars," KNMI, Tech. Rep. TR-355, Jan. 2016. [Online]. Available: cdn.knmi.nl/knmi/pdf/bibliotheek/knmipubTR/TR355.pdf
[6] S. M. Torres and D. A. Warde, "Ground clutter mitigation for weather radars using the autocorrelation spectral density," *J. Atmos. Oceanic Technol.*, vol. 31, no. 10, pp. 2049–2066, 2014.
[7] J. C. Hubbert, G. Meymaris, U. Romatschke, and M. Dixon, "Using a regression ground clutter filter to improve weather radar signal statistics: theory and simulations," *J. Atmos. Oceanic Technol.*, vol. 38, no. 8, pp. 1353–1375, 2021.
[8] M. Tahanout and J. Parent-du-Châtelet, "FILCOH – A novel technique to reduce ground clutter echoes in precipitation radars operating in multiple PRT," *IEEE Trans. Geosci. Remote Sens.*, vol. 59, no. 3, pp. 1967–1985, 2020.
[9] J. Aoyagi, "A study on the MTI weather radar system for rejecting ground clutter," *Pap. Meteor. Geophys.*, vol. 33, no. 4, pp. 187–243, 1983.
[10] J. Sugier, J. Parent du Châtelet, P. Roquain, and A. Smith, "Detection and removal of clutter and anaprop in radar data using a statistical scheme based on echo fluctuation," in *European Conf. on Radar in Meteorol. and Hydrol. (ERAD)*, Delft, Netherlands, 2002, pp. 17–24.
[11] I. Holleman and H. Beekhuis, "Review of the KNMI clutter removal," KNMI, Tech. Rep. TR-284, 2005. [Online]. Available: cdn.knmi.nl/knmi/pdf/bibliotheek/knmipubTR/TR284.pdf
[12] M.-H. Golbon-Haghighi, G. Zhang, and R. J. Doviak, "Ground clutter detection for weather radar using phase fluctuation index," *IEEE Trans. Geosci. Remote Sens.*, vol. 57, no. 5, pp. 2889–2895, 2019.
[13] J. C. Hubbert, M. Dixon, and S. M. Ellis, "Weather radar ground clutter. Part II: Real-time identification and filtering," *J. Atmos. Oceanic Technol.*, vol. 26, no. 7, pp. 1181–1197, 2009.
[14] P. Tabary, F. Guibert, L. Périer, and J. Parent-du-Châtelet, "An operational triple-PRT Doppler scheme for the French radar network," *J. Atmos. Oceanic Technol.*, vol. 23, no. 12, pp. 1645–1656, 2006.
[15] P. Tabary, "The new French operational radar rainfall product. Part I: Methodology," *Wea. Forecasting*, vol. 22, no. 3, pp. 393–408, 2007.
[16] R. J. Hogan, "Dual-Wavelength Radar Studies of Clouds," Ph.D. dissertation, University of Reading, Reading, UK, 1998.
[17] D. A. Warde and S. M. Torres, "Automatic detection and removal of ground clutter contamination on weather radars," in *Conf. on Radar Meteorology*, Williamsburg, VA, USA, Oct. 2009.
[18] C. Lubeigt, "Details on SIGMA integrals evaluation," 2025.
[19] D. S. Zrnić, "Simulation of weatherlike Doppler spectra and signals," *J. Appl. Meteorol. Clim.*, vol. 14, no. 4, pp. 619–620, 1975.